Quantum Capacitance in Nanoscale Device Modeling

D.L. John,[*] L.C. Castro, and D.L. Pulfrey[†]

Department of Electrical and Computer Engineering,

University of British Columbia, Vancouver, BC V6T 1Z4, Canada

(Dated: August 16, 2004)

Abstract

Expressions for the "quantum capacitance" are derived, and regimes are discussed in which this concept may be useful in modeling electronic devices. The degree of quantization is discussed for one- and two-dimensional systems, and it is found that two-dimensional (2D) metals, and one-dimensional (1D) metallic carbon nanotubes have a truly quantized capacitance over a restricted bias range. For both 1D and 2D semiconductors, a continuous description of the capacitance is necessary. The particular case of carbon nanotube field-effect transistors (CNFETs) is discussed in the context of one-dimensional systems. The bias regime in which the quantum capacitance may be neglected when computing the energy band diagram, in order to assist in the development of compact CNFET models, is found to correspond only to the trivial case where there is essentially no charge, and a solution to Laplace's equation is sufficient for determining a CNFET's energy band diagram. For fully turned-on devices, then, models must include this capacitance in order to properly capture the device behaviour. Finally, the relationship between the transconductance of a CNFET and this capacitance is revealed.

I. INTRODUCTION

The concept of "quantum capacitance" was used by Luryi[1] in order to develop an equivalent circuit model for devices that incorporate a highly conducting two-dimensional (2D) electron gas. Recently, this term has also been used in the modeling of one-dimensional (1D) systems, such as carbon nanotube (CN) devices.[2,3] Here, we derive expressions for this capacitance in one- and two-dimensions, showing the degree to which it is quantized in each case.

Our discussion focuses primarily on the 1D case, for which we use the carbon nanotube field-effect transistor (CNFET) as the model device, although the results apply equally well to other types of 1D semiconductors. The 2D case has been discussed in Ref. 1, and is included here only to illustrate key differences.

Equilibrium expressions are derived, and these are extended to cover two extremes in the non-equilibrium characteristic, namely: phase-coherent and phase-incoherent transport. In the former case, the wavefunction is allowed to interfere with itself, and may produce resonances depending on the structure of the device. This results in the charge, and the quantum capacitance, becoming strong functions of the length of the semiconductor. In the latter case, this type of resonance is not allowed, and the quantum capacitance is more uniform. Finally, we show how the quantum capacitance affects the transconductance of a CNFET, where the Landauer expression can be used to compute the current.[4]

II. EQUILIBRIUM QUANTUM CAPACITANCE

In order to derive analytical expressions, it is assumed that our device is in quasi-equilibrium, and that the carrier distribution functions are rigidly shifted by the local electrostatic potential. If the density of states (DOS) is symmetric with respect to the Fermi level, E_F, as in graphene, then we can write the charge density, Q, due to electrons and holes in the semiconductor, as

$$Q = q \int_0^\infty g(E) \left[f \left(E + \frac{E_G}{2} + qV_a \right) - f \left(E + \frac{E_G}{2} - qV_a \right) \right] dE, \qquad (1)$$

where q is the magnitude of the electronic charge, E is the energy, $g(E)$ is the 1D or 2D DOS, $f(E)$ is the Fermi-Dirac distribution function, V_a is the local electrostatic potential,

E_G is the bandgap, and E_F is taken to be mid-gap when $V_a = 0$. The quantum capacitance, C_Q, is defined as

$$C_Q = \frac{\partial Q}{\partial V_a}, \tag{2}$$

and has units of F/m^2 and F/m in the 2D and 1D cases, respectively.

A. Two Dimensions

In the two-dimensional case, if we employ the effective-mass approximation with parabolic bands, the DOS is given by

$$g(E) = \frac{m}{\pi\hbar^2}\nu(E), \tag{3}$$

where $\nu(E)$ is the number of contributing bands at a given energy, m is the effective mass, and $\hbar$ is Dirac's constant. If we combine this with Eqs. (1) and (2), and exchange the order of differentiation and integration, we get

$$C_Q = \frac{mq^2}{4\pi\hbar^2 kT}\int_0^\infty \nu(E)\left[\text{sech}^2\left(\frac{E + \frac{E_G}{2} - qV_a}{2kT}\right) + \text{sech}^2\left(\frac{E + \frac{E_G}{2} + qV_a}{2kT}\right)\right]dE, \tag{4}$$

where k is Boltzmann's constant, and T is temperature. If ν is a constant, we can perform the integration to get

$$C_Q = \frac{\nu mq^2}{2\pi\hbar^2}\left[2 - \frac{\sinh\left(\frac{E_G}{2kT}\right)}{\cosh\left(\frac{\frac{E_G}{2} - qV_a}{2kT}\right)\cosh\left(\frac{\frac{E_G}{2} + qV_a}{2kT}\right)}\right], \tag{5}$$

which reduces to

$$C_Q = \frac{\nu mq^2}{\pi\hbar^2}, \tag{6}$$

when $E_G = 0$ in agreement with Ref. 1, where metallic properties were assumed. Note that this function is quantized in the metallic case, but continuous for a semiconductor. For E_G greater than about $15kT$, however, the function makes a rapid transition from a small value to that given by Eq. (6) when V_a crosses $E_G/2$, and is thus effectively quantized.

B. One Dimension

In the one-dimensional, effective-mass case, we have

$$g(E) = \frac{\nu(E)}{\pi\hbar}\sqrt{\frac{2m}{E}}. \tag{7}$$

3

The explicit energy dependence of this DOS complicates the evaluation of our integral for C_Q. The approach suggested in Ref. 2, *i.e.*, using the fact that the derivative of $f(E)$ is peaked about E_F in order to approximate this integral using a Sommerfeld expansion,[5] cannot be done in general, due to the presence of singularities in the 1D DOS.

The capacitance is given by

$$C_Q = \frac{q^2}{2kTh}\sqrt{\frac{m}{2}}\int_0^\infty \frac{\nu(E)}{\sqrt{E}}\left[\mathrm{sech}^2\left(\frac{E+\frac{E_G}{2}-qV_a}{2kT}\right)+\mathrm{sech}^2\left(\frac{E+\frac{E_G}{2}+qV_a}{2kT}\right)\right]\mathrm{d}E\,, \quad (8)$$

where h is Planck's constant. For sufficiently large $|V_a|$, we can completely neglect one of the $\mathrm{sech}^2(\cdot)$ terms. As a simple example, if $V_a = 0.1\,\mathrm{V}$ for a material with $E_G \simeq 1\,\mathrm{eV}$, the contribution to the integral from the first term is roughly four orders of magnitude greater than the second. This approximation is equivalent to neglecting hole charge for positive V_a, and electron charge for negative V_a. The solid line in Fig. 1 shows the equilibrium C_Q as a function of V_a for a semiconductor with two valence and conduction bands: at 0.2 and $0.6\,\mathrm{eV}$ away from the Fermi level. An effective mass of $0.06m_0$ is assumed, where m_0 is the free-electron mass. The van Hove singularities, at each band edge, result in corresponding peaks in C_Q.

For a linear energy-wavevector relation, such as that near the Fermi level in graphene or a metallic CN, the DOS is constant. This is the case considered by Burke,[3] and is valid when V_a is such that $f(E)$ is approximately zero before the first van Hove singularity is encountered in the integral. Since the higher energy bands are not relevant to the integration under such a condition, ν is constant, and the DOS is given by

$$g(E) = \frac{2\nu}{hv_F}\,, \quad (9)$$

where v_F is the Fermi velocity. The result is

$$C_Q = \frac{2\nu q^2}{hv_F}\,, \quad (10)$$

which agrees with the expression quoted in Ref. 3.

Note that in Eq. (8) C_Q does not manifest itself as a multiple of some discrete amount, so "quantum capacitance" is not an appropriate description for a 1D semiconductor, unlike in the metallic 2D and metallic 1D CN cases, where the capacitance is truly quantized.

4

III.   GENERAL CONSIDERATIONS

We can now extend our discussion to include the non-equilibrium behaviour for a general, 1D, intrinsic semiconductor. All of the numerical results are based on the methods described in Refs. 6 and 7, which consider the cases when transport in the 1D semiconductor is either coherent or incoherent, respectively. While these methods were developed in order to describe CNFETs, their use of the effective-mass approximation allows them to be used for any device, and bias, where the semiconductor is described well by this approximation.

For phase-incoherent transport, we utilize a flux-balancing approach[7,8] to describe the charge in an end-contacted semiconductor. If we consider only the electrons that are far away from the contacts, $i.e.$, in the mid-length region, Eq. (1) becomes[8]

$$Q = -\frac{q}{2} \int_0^\infty g(E) T^*(E) \left[f\left(E + \frac{E_G}{2} - qV_a \right) \left(\frac{2}{T_R(E)} - 1 \right) \right.$$
$$\left. + f\left(E + \frac{E_G}{2} + q\left(V_{\text{bias}} - V_a \right) \right) \left(\frac{2}{T_L(E)} - 1 \right) \right] \mathrm{d}E \,, \tag{11}$$

where V_{bias} is the potential difference between the end contacts, $T_L(E)$ and $T_R(E)$ are the transmission probabilities at the left and right contacts respectively, $T^*(E) = T_L T_R / (T_L + T_R - T_L T_R)$ is the composite transmission probability for the entire system, and V_a is evaluated in the mid-length region. A similar expression holds for holes.

The first term in Eq. (11) resembles the equilibrium case, so we expect a similar form for that contribution to C_Q. The peak for each contributing band will occur at the same V_a, but the overall magnitude will be smaller due to the multiplication by the transmission function. The second term is also similar except that these peaks will now be shifted by V_{bias}. This is depicted by the dashed curve in Fig. 1, where the case illustrated by the solid curve has been driven from equilibrium by $V_{\text{bias}} = 0.2\,\text{V}$. Note the splitting of each large peak into two smaller peaks: one at the same point, and the other shifted by V_{bias}. Of course, the numerical value of the non-equilibrium capacitance depends on the exact geometry considered, as it will influence both V_a and the transmission probabilities in Eq. (11), but the trends shown here are general and geometry-independent.

For the coherent, non-equilibrium case, it is instructive to consider a metal-contacted device, in which the band discontinuities at the metal-semiconductor interfaces are sufficient to allow significant quantum-mechanical reflection of carriers even above the barrier. Further, we restrict our attention to short devices since the importance of coherence effects

is diminshed as the device length is increased. Due to the phase-coherence, then, we have a structure very much like a quantum well, even for devices where tunneling through the contact barriers is not important. For our device, we expect quasi-bound states to emerge at the approximate energies

$$E_n \simeq \frac{n^2\pi^2\hbar^2}{2mL^2},$$ (12)

where L is the semiconductor length. For $m \simeq 0.06m_0$, such as in a $(16,0)$ CN, $E_n \simeq 6.3(n/L)^2\,\text{eV}$, where L is in nanometres. This may be compared with the result for metallic CNs, where the linear energy-wavevector relationship yields a $1/L$ dependence.[3,9] Fig. 2(a) displays C_Q as a function of position and V_a for this choice of m. The maxima, indicated as brighter patches, show a dependence on V_a that reveals the population of quasi-bound states. Moreover, the maxima in position clearly show the characteristic modes expected from our simple square-well analogy. Note that the peak-splitting occurs for coherent transport as well, as shown in Fig. 2(b), where the peaks have been split by $V_{\text{bias}} = 0.1\,\text{V}$.

The main difference, between the coherent and incoherent cases, is the presence of the quasi-bound states. These serve to increase the number of C_Q peaks, since each quasi-bound state behaves like an energy band, and they also give rise to a strong spatial dependence. While Fig. 2 shows only a single-band, coherent result, inclusion of multiple bands would cause C_Q to exhibit peaks corresponding to each band, and to each quasi-bound state.

IV. APPLICATION: CNFETS

We now elaborate on the above in the context of CNFET modeling. In particular, for the purpose of developing compact models, it would be useful to ascertain the conditions under which the quantum capacitance is small in comparison with that due to the insulator geometry, a regime previously described as the "quantum capacitance limit."[2,10] To this end, we examine a coaxial CNFET, and treat V_a as the potential, with respect to the source contact, on the surface of the CN in the mid-length region. C_Q can be considered to be in series with the insulator capacitance, C_{ins},[11] however, the ratio of these capacitances is related not to V_a and the gate-source voltage, V_{GS}, but to $\partial V_{GS}/\partial V_a$. If the charge accumulation were linear over some bias range, as might be deemed appropriate at the local extrema of C_Q, we could relate this ratio directly to the potentials.

Knowledge of the "C_Q limit" is beneficial since a relatively low C_Q implies that changes

in V_a will closely track changes in V_{GS}, obviating the need to calculate C_Q when computing the energy band diagram. Note, however, that C_Q cannot be neglected when considering performance metrics that depend on the total capacitance, *e.g.*, the propagation delay may be dominated by C_Q in this limit. We find that $C_Q \ll C_{\text{ins}}$ only when Q is small enough as to allow for the employment of a Laplace solution[12] for the position-dependent potential: eliminating the need for a cumbersome self-consistent Schrödinger-Poisson solution. The difference between these solutions is illustrated in Fig. 3 for a coaxial CNFET with an insulator thickness and CN radius of 2.5 and 0.6 nm, respectively, and an end contact work function that is 0.6 eV less than that of the CN. Figs. 3(a) and (b) correspond to the off and turn-on states, respectively. While equilibrium band diagrams are shown for simplicity, similar trends prevail with the application of a drain-source voltage. For a device dominated by thermionic emission, such as the one depicted here, the disagreement shown in (a), close to the contacts, will not significantly affect the current calculation, while in (b), the error would clearly be much greater. For a device dominated by tunneling, *i.e.*, if the energy bands had the opposite curvature, a similar discrepancy would result in a large error in the current calculations due to the exponential dependence of the tunneling probability on the barrier shape.

Now, we seek to theoretically quantify the condition under which $C_Q \ll C_{\text{ins}}$. From Fig. 1, we see that the first local maxima is on the order of 0.3 nF/m. For this peak to be insignificant, we would require C_{ins} to be orders of magnitude higher than this. For a 2 nm-thick dielectric in a coaxial device, we would require a relative permittivity of ~ 530 in order to give two orders of magnitude difference between C_{ins} and C_Q. Reports of solid, high-permittivity dielectrics for CN devices[13–16] have quoted values only as high as 175 for the relative permittivity,[16] so we conclude that, for realistic dielectrics, we can expect to only marginally enter the C_Q limit, and that the first C_Q peak will be significant. If we consider an electrolytically-gated CNFET,[17] we could perhaps achieve a relative permittivity of 80, and an effective thickness of 1 nm, as considered in Ref. 2, but this would yield $C_{\text{ins}} \simeq 25 C_Q$, and would, again, only marginally be entering this limit.

For a short-channel, phase-coherent device, the requirement for negligible C_Q is that the Fermi levels for the injecting contacts should be far away from $E_1 \simeq 6.3/L^2$ eV. If we consider positive applied voltages to the gate and drain, this would imply that qV_a should be more than about $5kT$ below $E_G/2 + E_1$. For the long-channel or phase-incoherent cases,

this condition is given by $E_1 = 0$, corresponding to the conduction band edge. The relative importance of C_Q, computed in the mid-length region of the device, is depicted in Fig. 4 for a phase-incoherent device as a function of V_{GS} and the drain-source voltage, V_{DS}, where we note that V_{DS} corresponds to V_{bias}, and that V_a is influenced by both V_{DS} and V_{GS}. Here, the aforementioned peak-splitting for non-zero V_{DS} is clearly evident in the diverging bright lines. Only for low bias voltages can C_Q be neglected, as shown by the black region in the centre of the figure. However, this figure also reveals the regions where it becomes approximately constant, i.e., the bias ranges where the series capacitance relationship can be used to estimate V_a from V_{GS}.[11] Note, though, that this is a single-band calculation, and these regions may not be as prevalent when higher transverse modes are considered.

Finally, we consider the influence of C_Q on the transconductance for our model device, which has a doubly-degenerate lowest band. If we employ the Landauer equation[4] for transport in two conducting channels, the current is

$$I = \frac{4q}{h} \left\{ \int_{E_C}^{\infty} T_n(E) \left[f(E) - f(E + qV_{DS}) \right] \mathrm{d}E \right.$$
$$\left. - \int_{-\infty}^{E_V} T_p(E) \left[f(E) - f(E - qV_{DS}) \right] \mathrm{d}E \right\}, \tag{13}$$

where $E_C = E_G/2 - qV_a$ is the spatially constant conduction band edge in the mid-length region of a long-channel device, $E_V = E_C - E_G$ is the valence band edge, and $T_n(E)$ and $T_p(E)$ are the transmission probabilities for electrons and holes, respectively, from one end contact to the other. The transconductance is defined as

$$g_m = \frac{\partial I}{\partial V_{GS}}, \tag{14}$$

which yields

$$g_m = \frac{4q^2}{h} \left[\frac{C_{\mathrm{ins}}}{C_Q + C_{\mathrm{ins}}} \right] \left\{ T_n(E_C) \left[f(E_C) - f(E_C + qV_{DS}) \right] \right.$$
$$\left. - T_p(E_V) \left[f(E_V) - f(E_V - qV_{DS}) \right] \right\}. \tag{15}$$

Note that, if we assume only electron transport with $C_Q \ll C_{\mathrm{ins}}$, low temperature, and high V_{DS}, this expression reduces to the classic Landauer result[4] for two conducting channels

$$g_m = \frac{4q^2}{h} T_n, \tag{16}$$

which is the ultimate transconductance in this case.[7,10] Fig. 5(a) shows the theoretical transconductance, from Eq. (15), for our model device, while (b) and (c) show the energy-distribution term (in curly braces), and the capacitance ratio term (in square brackets),

respectively. The decrease in g_m, at high V_{GS}, is due primarily to the decreasing difference in the contact distribution functions as, for example, E_C becomes closer to qV_{DS}. However, the exact magnitude of g_m is dependent on the capacitance ratio. Further, C_Q will be responsible for additional oscillations in g_m, as observed experimentally in Ref. 18 for example, if higher bands, or quasi-bound states, are considered in the calculation. Such transconductance features have also been predicted in Ref.[19].

V.   CONCLUSION

From this theoretical study on the charge-voltage relationship in one- and two-dimensional systems, it can be concluded that:

1. the "quantum capacitance" occurs in discrete quanta for 2D and 1D metals if V_a is such that the Fermi level falls in a linear portion of the energy-wavevector relationship;

2. for 2D semiconductors, this capacitance is approximately quantized if the bandgap is greater than about $15kT$, and varies continuously otherwise;

3. for long, 1D systems with parabolic bands, and with V_a such that these bands contribute to the charge density, the equilibrium capacitance exhibits maxima that are related to the number of contributing bands at a given energy;

4. application of a bias to a 1D semiconductor causes each equilibrium capacitance peak to split into two smaller peaks, with one remaining at the equilibrium position, and the other shifting by the applied bias;

5. the potential in the mid-length region of a 1D semiconductor cannot be computed, in general, from potential division due to two capacitors in series due to the nonlinearity of C_Q;

6. for short, phase-coherent structures, the quasi-bound states cause the capacitance peaks to occur at higher local electrostatic potentials, with additional maxima corresponding to the occupation of these states;

7. for a CNFET, it is unlikely that the insulator capacitance can become high enough to allow the quantum capacitance to be neglected in energy band calculations, except

in cases where the accumulated charge is low enough that the solution to Laplace's equation is sufficient for the calculation, or if extremely high permittivity dielectrics are used;

8. the quantum capacitance has a significant effect on the transconductance, and should be considered when modeling CNFETs.

ACKNOWLEDGMENTS

REFERENCES

---

[*] Electronic address: davej@ece.ubc.ca

[†] Electronic address: pulfrey@ece.ubc.ca

[1] Serge Luryi, Appl. Phys. Lett. **52**(6), 501 (1988).

[2] Anisur Rahman, Jing Guo, Supriyo Datta, and Mark S. Lundstrom, IEEE Trans. Electron Devices **50**(9), 1853 (2003).

[3] P. J. Burke, IEEE Trans. Nanotechnol. **2**(1), 55 (2003).

[4] David K. Ferry and Stephen M. Goodnick, *Transport in Nanostructures* (Cambridge University Press, New York, 1997).

[5] Neil W. Ashcroft and N. David Mermin, *Solid State Physics* (Harcourt College Publishers, New York, 1976), 1st edn.

[6] D. L. John, L. C. Castro, P. J. S. Pereira, and D. L. Pulfrey, in *Proc. NSTI Nanotech* (2004), vol. 3, pp. 65–68.

[7] L. C. Castro, D. L. John, and D. L. Pulfrey, Nanotechnology (2004). Submitted. [Online.] Available: http://nano.ece.ubc.ca/pub/publications.htm.

[8] L. C. Castro, D. L. John, and D. L. Pulfrey, in *Proc. IEEE COMMAD* (2002), pp. 303–306.

[9] Zhen Yao, Cees Dekker, and Phaedon Avouris, in *Carbon Nanotubes*, edited by Mildred S. Dresselhaus, Gene Dresselhaus, and Phaedon Avouris (Springer-Verlag, Berlin, 2001), vol. 80 of *Topics Appl. Phys.*, pp. 147–171.

[10] L. C. Castro, D. L. John, and D. L. Pulfrey, in *Proc. SPIE Int. Microelectronics, MEMS and Nanotechnology Symp.* (2003). [Online.] Available: http://nano.ece.ubc.ca/pub/publications.htm.

[11] Jing Guo, Sebastien Goasguen, Mark Lundstrom, and Supriyo Datta, Appl. Phys. Lett. **81**(8), 1486 (2002).

[12] S. Heinze, M. Radosavljević, J. Tersoff, and Ph. Avouris, Phys. Rev. B **68**, 235418 (2003).

[13] Adrian Bachtold, Peter Hadley, Takeshi Nakanishi, and Cees Dekker, Science **294**, 1317 (2001).

[14] J. Appenzeller, J. Knoch, V. Derycke, R. Martel, S. Wind, and Ph. Avouris, Phys. Rev. Lett. **89**(12), 126801 (2002).

[15] Ali Javey, Hyoungsub Kim, Markus Brink, Qian Wang, Ant Ural, Jing Guo, Paul McIntyre, Paul McEuen, Mark Lundstrom, and Hongjie Dai, Nature Mater. **1**, 241 (2002).

[16] B. M. Kim, T. Brintlinger, E. Cobas, M. S. Fuhrer, Haimei Zheng, Z. Yu, R. Droopad, J. Ramdani, and K. Eisenbeiser, Appl. Phys. Lett. **84**(11), 1946 (2004).

[17] Sami Rosenblatt, Yuval Yaish, Jiwoong Park, Jeff Gore, Vera Sazonova, and Paul L. McEuen, Nano Lett. **2**(8), 869 (2002).

[18] Minkyu Je, Sangyeon Han, Ilgweon Kim, and Hyungcheol Shin, Solid-State Electron. **44**, 2207 (2000).

[19] D. Jiménez, J. J. Sáenz, B. Iñíguez, J. Suñé, L. F. Marsal, and J. Pallarès, IEEE Electron Device Lett. **25**(5), 314 (2004).

FIGURES

Fig. 1. 1D quantum capacitance as a function of the local electrostatic potential at equilibrium (solid), and for the mid-length region of an end-contacted semiconductor with a bias voltage of $0.2\,V$ (dashed) between the end contacts. The effective mass is taken to be $0.06m_0$, and energy bands are situated at 0.2 and $0.6\,eV$ on either side of the Fermi level.

Fig. 2. 1D quantum capacitance, in arbitrary units, for a short-channel, phase-coherent semiconductor as a function of position and the local electrostatic potential for applied bias voltages of (a) 0 and (b) $0.1\,V$ between the end contacts. The bright areas indicate higher capacitance.

Fig. 3. Comparison of the equilibrium energy band diagrams, for a model CNFET, at gate-source voltages of (a) 0.2 and (b) $0.32\,V$, computed via the solutions to a self-consistent Schrödinger-Poisson system (solid), and to Laplace's equation (dashed). The Fermi energy is at $0\,eV$.

Fig. 4. Quantum capacitance for a long-channel CNFET as a function of the gate- and drain-source voltages. Numerical values are displayed as a fraction of the insulator capacitance.

Fig. 5. (a) Electron transconductance for a model CNFET as a function of the gate-source voltage for drain-source voltages of 0.2 (solid) and $0.4\,V$ (dashed). Constituent elements of the theoretical transconductance from Eq. (15) are (b) the energy-distribution term (in curly braces), and (c) the capacitance-ratio term (in square brackets).
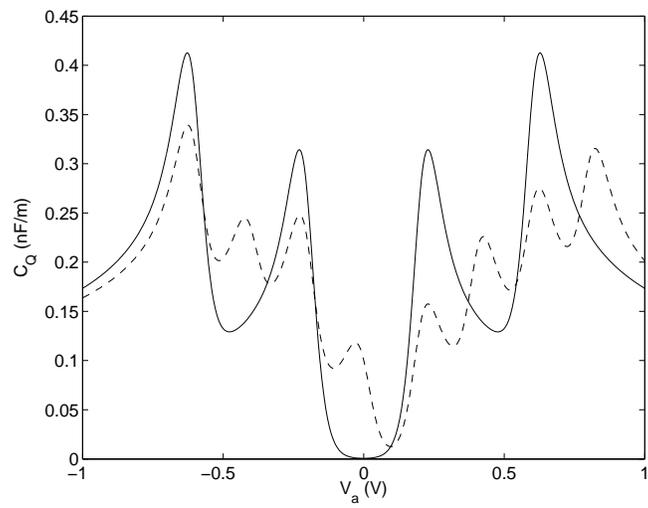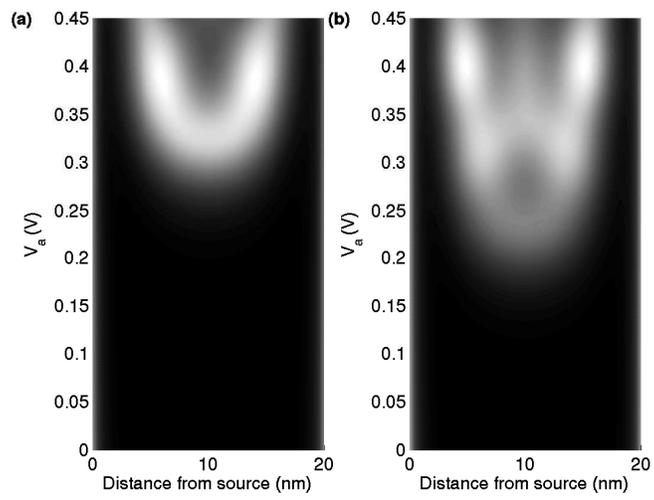
13

FIG. 1: D. L. John, J. Appl. Phys.

(a)

(b)

V_a (V)

Distance from source (nm)

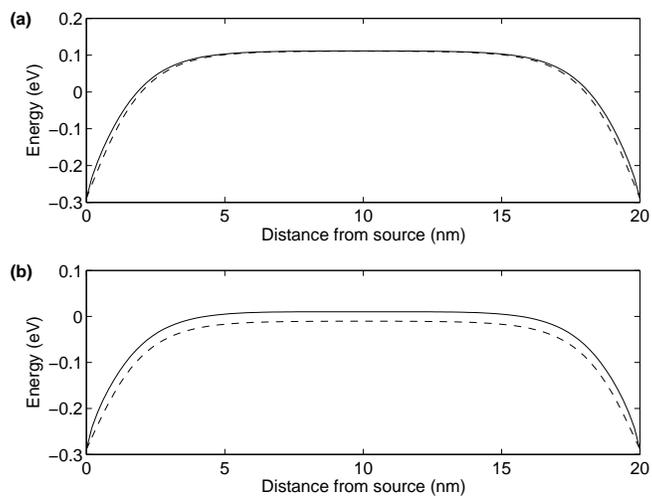FIG. 2: D. L. John, J. Appl. Phys.
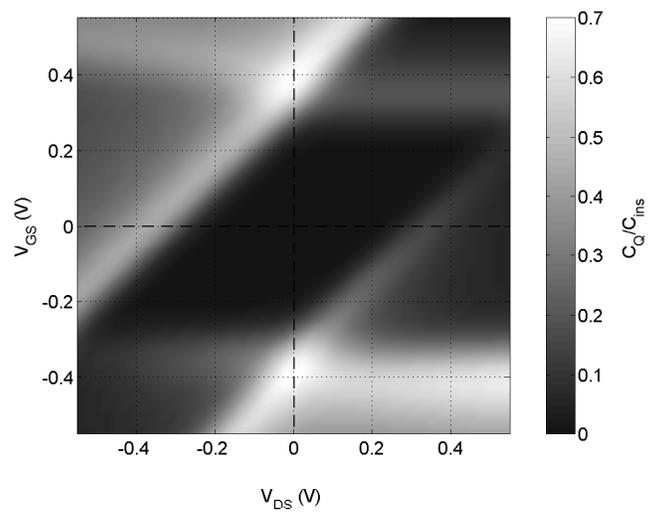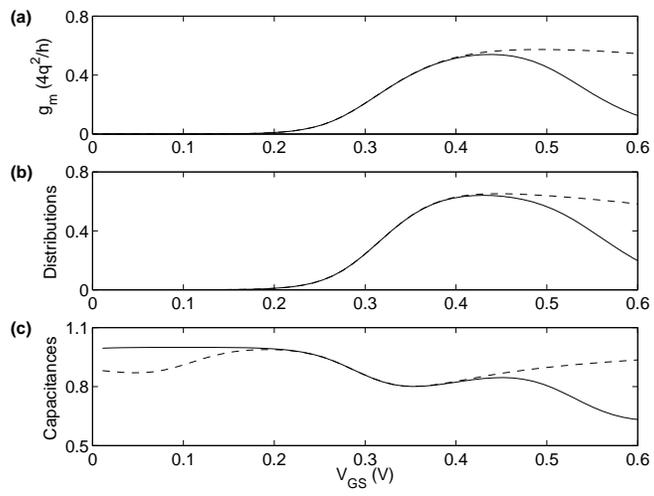
15

FIG. 3: D. L. John, J. Appl. Phys.

FIG. 4: D. L. John, J. Appl. Phys.

FIG. 5: D. L. John, J. Appl. Phys.